

Analysis of notch depth and loading rate effects on crack growth in concrete by FE and DIC

Xiangyi Zhu¹, Xudong Chen^{*2}, Jun Lu³ and Xiangqian Fan³

¹College of Water Conservancy and Hydropower Engineering, Hohai University, Nanjing 210098, China

²College of Civil and Transportation Engineering, Hohai University, Nanjing 210098, China

³Department of Materials and Structural Engineering, Nanjing Hydraulic Research Institute, Nanjing, 210024, China

(Received April 16, 2019, Revised November 13, 2019, Accepted November 15, 2019)

Abstract. In this paper, the fracture characteristics of concrete specimens with different notch depths under three-point flexural loads are studied by finite element and fracture mechanics methods. Firstly, the concrete beams (the size is 700×100×150 mm) with different notch depths ($a=30$ mm, 45 mm, 60 mm and 75 mm respectively) are tested to study the influence of notch depths on the mechanical properties of concrete. Subsequently, the concrete beams with notch depth of 60 mm are loaded at different loading rates to study the influence of loading rates on the fracture characteristics, and digital image correlation (DIC) is used to monitor the strain nephogram at different loading rates. The test results show that the flexural characteristics of the beams are influenced by notch depths, and the bearing capacity and ductility of the concrete decrease with the increase of notch depths. Moreover, the peak load of concrete beam gradually increases with the increase of loading rate. Then, the fracture energy of the beams is accurately calculated by tail-modeling method and the bilinear softening constitutive model of fracture behavior is determined by using the modified fracture energy. Finally, the bilinear softening constitutive function is embedded into the finite element (FE) model for numerical simulation. Through the comparison of the test results and finite element analysis, the bilinear softening model determined by the tail-modeling method can be used to predict the fracture behavior of concrete beams under different notch depths and loading rates.

Keywords: finite elements; notch depths; loading rates; digital image correlation (DIC); tail-modeling method; fracture energy

1. Introduction

For the last few years, the number and size of concrete structures are both increasing with the acceleration of urbanization all over the world. However, as a kind of quasi-brittle material, concrete has some shortcomings, such as poor toughness, low tensile strength and difficult control of crack width after cracking, which make it difficult for many concrete structures to avoid the natural defects such as micro-cracks, micro-pore and so on (Reinhardt and Reinhardt 1986, Duan *et al.* 2006). Moreover, the length, shape and distribution of these cracks are random, which greatly affects the safety and service life of concrete structures. Haeri and his team have done a lot of researches in this field, and they thought that these crack characteristics (number, length, shape, distribution and so on) have a strong influence on the breaking path and determined the carrying capacity of the structures (Haeri *et al.* 2013, Haeri 2015, Haeri and Sarfarazi 2016, Sarfarazi and Haeri 2016). Different notch depths will have a significant impact on the development of cracks in concrete under three-point flexural loads (Ohno *et al.* 2014, Karamloo and Mazloom 2018), and the development of

cracks indirectly affects the ultimate load and deflection of concrete structures. Therefore, it is necessary to study the influence of different notch depths on the mechanical properties of concrete from the perspective of fracture mechanics, so as to ensure the safe operation of concrete structures.

Meanwhile, researchers all over the world have been studying the influence of loading rates on the mechanical properties of concrete (Reinhardt and Ozbolt 2007, Travas *et al.* 2009, Yan *et al.* 2009, Shang and Song 2013). For example, the compressive strength of the concrete increases with the increase of the loading rates. In addition to compressive strength, loading rate also affects other properties of the concrete. Zhang *et al.* (2014) obtained that the fracture energy and flexural strength increase by 152% and 248% with the increase of loading rate from 10^{-3} mm/s to 10^3 mm/s. Ranade *et al.* (2015) found that the tensile strength and cracking strength increased by 42% and 53% with the increase of the strain rate from 10^{-4} /s to 10/s. Although many researchers have done a lot of research on the influence of the loading rates on concrete performance, most of them use traditional test methods to analyze the influence of loading rate on the concrete. As a full-field optical technology, digital image correlation (DIC) can visually display the development of cracks. Some researchers have successfully obtained the bond fracture behavior of the concrete by DIC (Ali-Ahmad *et al.* 2006, Subramaniam *et al.* 2007, Carloni and Subramaniam 2010,

*Corresponding author, Professor
E-mail: cxdong1985@hotmail.com

Table 1 The mixture proportion of materials used in the experiment

Material consumption (kg/m ³)					Plasticizer (kg/m ³)
Cement	Water	Fly ash	Gravel	Sand	
358	177	90	1209.8	919.4	4.31

2013). Robins (2001) and Subramaniam (2015) tried to study the crack growth of the concrete by using DIC. Li (2018) also used DIC to study the crack shape of concrete beam under three-point flexural load. Therefore, it is necessary to explore the internal cause of the influence of loading rate on mechanical properties and fracture characteristics of concrete by DIC.

For the concrete, the fracture process is the most basic phenomenon (Skarzynski *et al.* 2015). Fracture mechanics and fracture energy due to the development of cracks in concrete have been paid much attention in practical engineering (Firoozi *et al.* 2018). Fracture mechanics is a kind of research sciences on the damage of concrete structure due to crack development and expansion according to the energy criterion (Abbass *et al.* 2013). However, due to the obvious size effect of concrete in fracture failure, the use of fracture mechanics in concrete structure design can well monitor the damage degree of concrete components (Elices *et al.* 1997). This fracture process is accompanied by the development of various main cracks, secondary cracks and micro-cracks, which makes this process extremely complex (Bažant and Planas 1997). In order to study the fracture behavior of concrete more intuitively and effectively, many researchers have combined laboratory tests with numerical simulation to achieve the purpose of research (Navalurkar and Hsu 2001, Xiao *et al.* 2012, Trivedi and Singh 2015, Earij *et al.* 2017, Chen *et al.* 2017, Rama *et al.* 2017, Gang and Kwak 2017, Sasmal *et al.* 2018). As an effective tool, numerical simulation can make up for the shortage of laboratory research. Therefore, it is necessary to study the fracture process of concrete by non-linear finite element (ABAQUS) to ensure the safety of concrete structure.

In this paper, the influence of notch depths and loading rates on crack growth in concrete is studied by means of experimental tests, theoretical model and numerical simulation. The digital image correlation (DIC) is used to monitor the strain nephogram in the tests, and the tail-modeling method is presented to accurately determine the bilinear softening constitutive model which is embedded into the finite element model for predicting the fracture characteristic of the concrete beams under different notch depths and loading rates. This research is of great significance to ensure the safe operation of concrete structure.

2. Experimental plan

The raw materials and mixture proportion of the plain concrete beams are listed in Table 1. The materials used in this experiment include gravel whose maximum particle size is 20 mm, sand whose density is 2600 kg/m³, fly ash



Fig. 1 The slump test of fresh concrete

Table 2 The basic mechanical properties of the concrete

Material property	Unit	Value	Std.dev.
Compressive strength f_c	MPa	46.13	0.23
Tensile strength f_t	MPa	2.96	0.14
Elastic Modulus E	GPa	33.50	0.09
Poisson's ratio ν		0.15	0.04

and CEM I 42.5R Portland. The water-cement ratio and sand content were 0.40 and 43.2% respectively. In order to evaluate the working performance of cast-in-situ concrete, the collapsed slump of the concrete is tested, as shown in Fig. 1. The slump of cast-in-place concrete measured in the laboratory is 180 mm. The test results show that the plain concrete in this experiment can meet the normal workability.

The size of standard specimens used in the three-point flexural test is 700×100×150 mm, and the notch depths (a) are 75 mm, 60 mm, 45 mm and 30 mm, respectively. The specimens are cast for four batches, and each batch consists of eleven beams for three-point flexural test and five standard cubic specimens with 150×150×150 mm for compressive test. These cubic specimens are used to test the compressive strength of each batch of plain concrete after curing for 28 days. After casting for 24 hours, all the specimens are demoulded and put in the water for curing. All the beams are cured in the water for at least 60 days until the three-point flexural tests are carried out in order to avoid the enhancement of the strength of the concrete beams in the air. The mean value of compressive strength after 28d is 46.13 MPa. Other basic mechanical properties of the concrete are listed in Table 2.

The test is mainly aimed at studying the influence of notch depth and loading rate on crack growth and determining the corresponding fracture energy. The three-point flexural tests are carried out on the MTS testing machine. The loading is controlled by displacement and the span is 600 mm. Meanwhile, the loading rate is set as 0.010 mm/s, 0.002 mm/s and 0.0002 mm/s in order to study the influence of loading rate on the mechanical properties and fracture characteristics of the concrete specimens. The details of each test condition are shown in Table 3. L , b and h represent the length, width and height of the concrete specimen respectively. In order to calculate the fracture

Table 3 The details of each test condition

Test No.	Specimen type	L (mm)	b (mm)	h (mm)	a (mm)	Loading rate (mm/s)
1	TPB-30	700	100	150	30	0.002
	TPB-45	700	100	150	45	0.002
	TPB-60	700	100	150	60	0.002
	TPB-75	700	100	150	75	0.002
2	TPB-60-1	700	100	150	60	0.010
	TPB-60-2	700	100	150	60	0.002
	TPB-60-3	700	100	150	60	0.0002

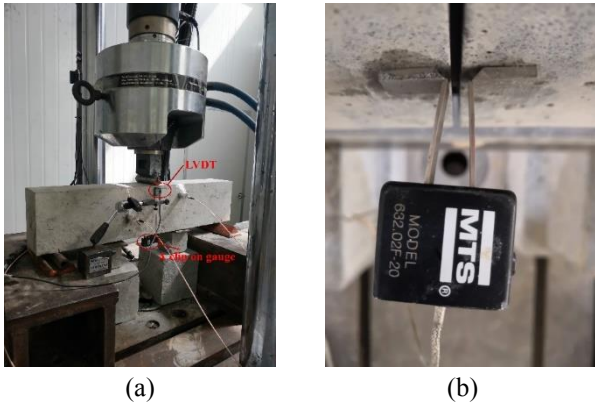


Fig. 2 (a) The flexural experiment setup, (b) The detail of the clip-on gauge

energy, the linear variable differential transformer (LVTD) was used to monitor the deflection (δ) of the upper part of the notch in the middle span of concrete beams, as shown in Fig. 2(a). At the same time, the crack mouth opening displacement (CMOD) of concrete specimens was measured by a clip-on gauge, and the relationship curve between the load and CMOD was monitored. The detail of the clip-on gauge is shown in Fig. 2(b).

For studying the influence of the loading rates on the peak load and fracture characteristics of the concrete more intuitively, the strain nephogram of different loading stages at different loading rates was monitored by DIC technique. In this study, the commercial software PMLAB DIC-3D was used for image correlation analysis. The camera resolution is 2048×2248 pixels, and the subset size is 29×29 pixels. There are regular intervals in the reference image in the form of the grid. The resolution of the system depends on the size of the observation area. In this test, the actual size of each pixel obtained according to the observation area is about 0.07 mm, while the relative error of the calibrated system is 0.02 pixels, namely 1.4 microns. The accuracy of strain measurement is 10 microstrains. In order to obtain a random pattern, speckle patterns of black and white paint were sprayed onto the surface of specimens, as shown in Fig. 3(b). And the surface images of the specimens were taken by two cameras, which were placed above the notch where the cracks might develop. The central part of the concrete beam was photographed, as shown in Fig. 3(a).

3. Test results and analysis



(a)



(b)

Fig. 3 (a) The DIC experiment setup, (b) The concrete beams after failure

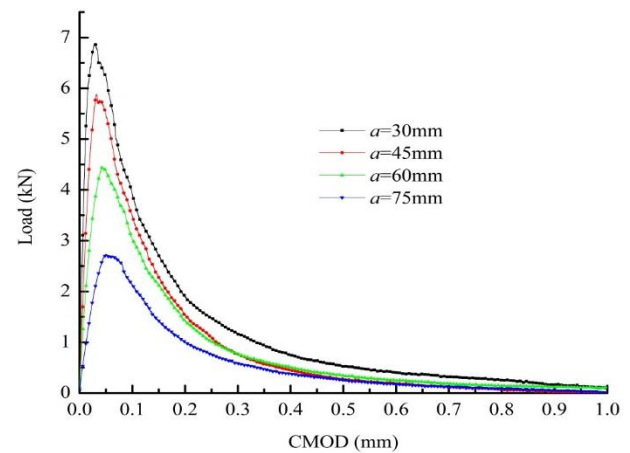


Fig. 4 Load-CMOD curves of concrete beams with different notch depths

3.1 Effect of notch depth on fracture characteristics

According to the linear elastic limit theory, it will break regardless of its size when the concrete specimen reaches the ultimate stress or strain. According to this assumption, the flexural strength of concrete beams is determined by elastic ultimate to predict the peak load of the concrete. Due to the influence of the notch, there are some limitations in this method. Hence, it is particularly necessary to quantify the effect of notch depth on concrete performance. For determining the influence of notch depth on fracture characteristics of the concrete, the loading rate is set to a constant value of 0.002 mm/s and the three-point flexural test is carried out on the plain concrete beams with different notch depths (30 mm, 45 mm, 60 mm and 75 mm) by MTS.

The relationships curves between CMOD and the load at different notch depths (a) are plotted in Fig. 4. It can be

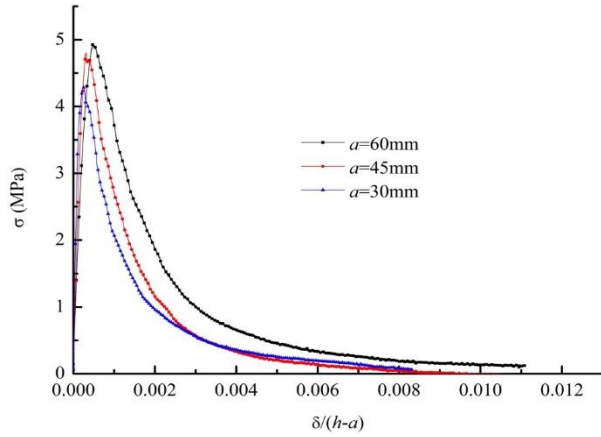


Fig. 5 Relationship between nominal stress and relative displacement of concrete beams with different notch depths

concluded from the Load-CMOD curve that the peak load decreases with the increase of the notch depth. When the notch depth is 30 mm, the flexural peak load of the concrete specimen reaches 6.89 kN. When the notch depth is 60 mm, the peak load is reduced to 4.44 kN, and the bearing capacity is reduced by 35.6%. The limit deformation and peak load of concrete specimens decrease with the increase of the notch depth. In the post-peak stage, the load drop amplitude gradually increases with the increase of notch depth. It can be seen that different notch depths have a significant impact on concrete strength. The Load-CMOD curve intuitively proves that the flexural behavior of the concrete specimens under three-point flexural load is affected by notch depth, while the ductility and bearing capacity decrease with the increase of the notch depth.

For studying the influence of notch depth on nominal stress, the plain concrete specimens with different notch depths are tested, and the nominal stress (at any stage of loading) can be calculated by the Eq. (1).

$$\sigma = \frac{3Ps}{2b(h-a)^2} \quad (1)$$

where P is the load of the concrete beam, s is the span, b and h are the width and height respectively, and a is the notch depth.

Fig. 5 shows the relationship between nominal stress and the ratio of vertical displacement (deflection δ) to effective height ($h-a$) of concrete beams. It can be seen from the curve that the ultimate nominal stress of concrete samples gradually increases with the increase of the notch depth, which also proved the influence of notch depth on concrete strength. However, this is not related to the increase of the strength of the material itself, but a limitation for the linear elastic calculation of concrete stress state.

For studying the influence of notch depth on ultimate nominal stress of the concrete more intuitively, the relationship curve between effective height ($h-a$) and ultimate nominal stress (σ_{Nu}) is plotted in Fig. 6. It can be seen from the curve that the concrete beams in the test have a statistically significant (95% confidence level) notch effect on the ultimate nominal stress. The bigger the notch

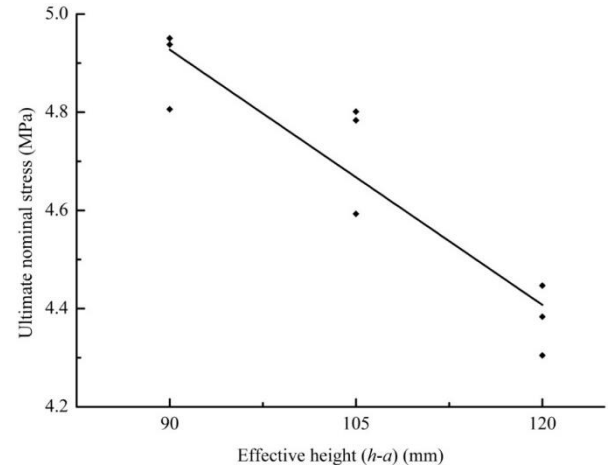


Fig. 6 The influence of notch depth on ultimate nominal stress (σ_{Nu})

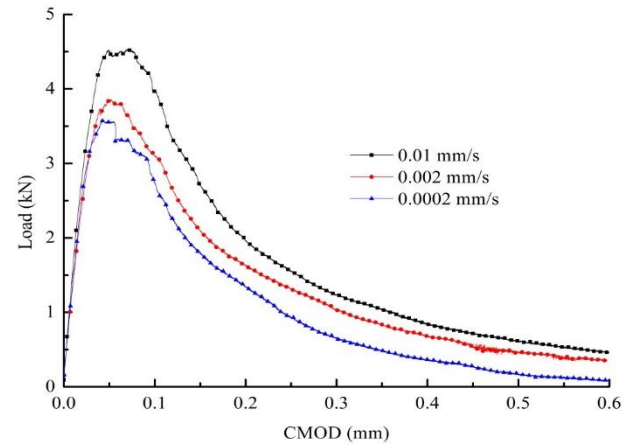


Fig. 7 Load-CMOD curves of concrete beams at different loading rates

depth is, the greater the tensile stress is in the upper region of the notch. The tested concrete specimens have the same properties except the notch depth, and this indicates that the ability to bear flexural stress at any point on the concrete specimen is the same. However, the final test results show that the concrete specimen will be destroyed under the relatively small flexural stress when the notch depth is relatively small. This further confirms that the strength of the concrete is greatly affected by notch depth.

3.2 Effect of loading rate on fracture characteristics

For studying the effect of different loading rates on the peak load of the concrete, three-point flexural tests are carried out on concrete beams with the same crack depth ($a=60$ mm) under different loading rates (0.010 mm/s, 0.002 mm/s and 0.0002 mm/s respectively), as shown in Table 3. The Load-CMOD curves obtained from the tests are shown in Fig. 7. It can be concluded from the curve that the peak load gradually decreases with the decrease of loading rate. When the loading rate is 0.010 mm/s, the peak load is about 4.5 kN. When the loading rate drops to 0.0002 mm/s, the peak load is about 3.6 kN, which decreases by about 20%. It can be seen that the loading rate has a

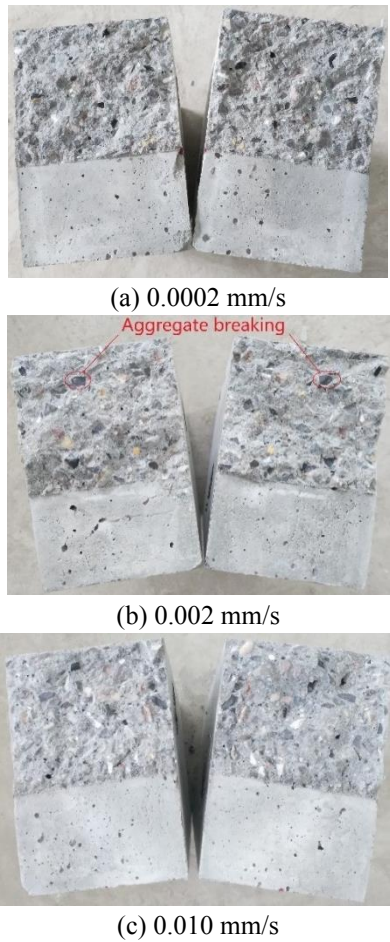


Fig. 8 The failure sections of concrete beams at different loading rates

considerable influence on the peak load of concrete. Therefore, the influence of the loading rates on the peak load of the concrete is considerable.

The failure sections of concrete beams at different loading rates are shown in Fig. 8. It can be seen from the figure that the failure section is uneven when the loading rate is low, and the flatness of the failure section increases with the increase of loading rate. This is mainly because the failure time of concrete beams is longer when the loading rate is lower. During this period, the cracks generated by loading will extend along the weakest area around the interface transition zone. However, the loading period is shorter when the loading rate is higher, and the cracks will spread directly through the aggregate. The strength and toughness of the aggregate are generally higher than that of interface transition zone, which is the main reason for the higher strength of concrete beams at higher loading rate.

Fig. 9-Fig. 11 show the comparison of strain nephogram of different loading stages monitored by DIC at different loading rates. It can be seen from the figures that strain localization is obvious at pre-peak loading stage. Furthermore, as the loading stage progressively moves backward, the single visible crack gradually develops on the upper part of the notch. The increase of crack length is obviously related to the softening of post-peak loading response, and the crack opening displacement gradually

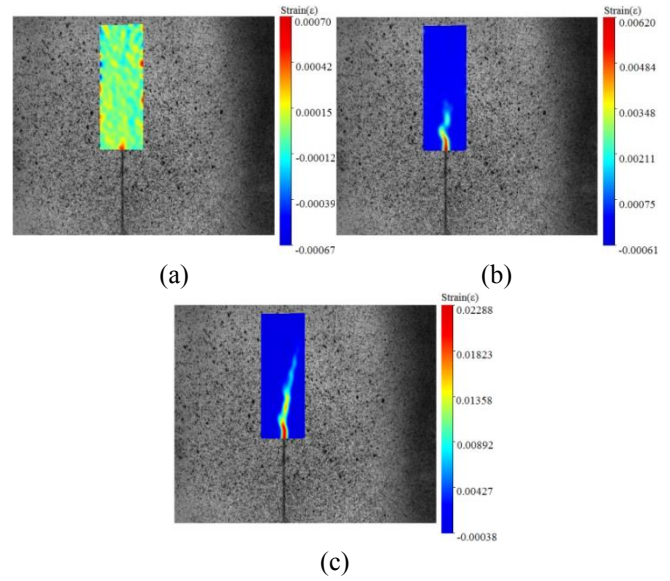


Fig. 9 The strain nephogram of different loading stages monitored by DIC when the loading rate is 0.010 mm/s: (a) 80% P_{max} at pre-peak stage; (b) 100% P_{max} ; (c) 80% P_{max} at post-peak stage

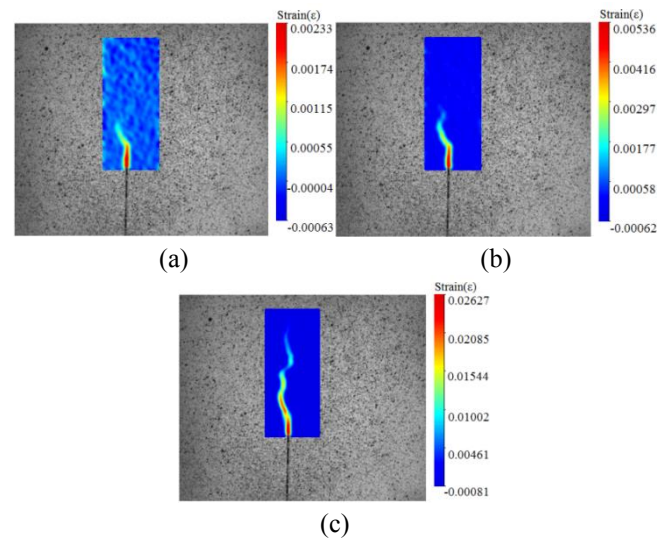


Fig. 10 The strain nephogram of different loading stages monitored by DIC when the loading rate is 0.002 mm/s: (a) 80% P_{max} at pre-peak stage; (b) 100% P_{max} ; (c) 80% P_{max} at post-peak stage

increases with the expansion of cracks on the upper part of the notch. When the loading rate is high, the cracks tend to develop along a straight line (as shown in Fig. 9), which is due to the short loading period and the tendency of the cracks to propagate through the aggregate directly. The crack develops along a curve with little curvature when the loading rate decreases to 0.002 mm/s, and the curvature of the propagation direction of the crack increases further when the loading rate decreases to 0.0002 mm/s. This is mainly due to the fact that the cracks spread along the weakest area around the interface transition zone when the concrete beam is broken for a long time. It is consistent with the above analysis of the failure section of concrete

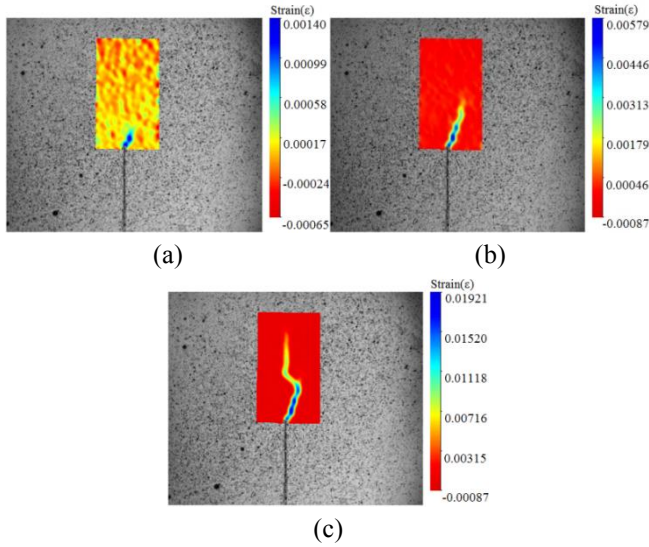


Fig. 11 The strain nephogram of different loading stages monitored by DIC when the loading rate is 0.0002 mm/s: (a) 80% P_{\max} at pre-peak stage; (b) 100% P_{\max} ; (c) 80% P_{\max} at post-peak stage

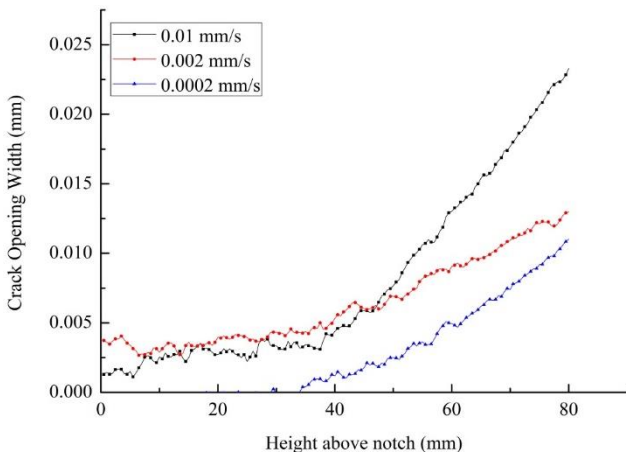


Fig. 12 Crack opening width as a function of height above the notch for different loading rates at 100% P_{\max}

beams.

Fig. 12 studies the crack opening width at different heights above the notch under different loading rates. It can be concluded from the curve that the crack opening width increases significantly when the loading rate increases. The crack opening width of concrete beam is 0.023 mm at 80 mm above the notch when the loading rate is 0.01 mm/s. The crack opening widths at loading rates of 0.002 mm/s and 0.0002 mm/s are 0.013 mm and 0.011 mm respectively, which are 43.5% and 52.2% smaller than that at loading rates of 0.01 mm/s. The larger the crack opening width is, the larger the energy and the peak load are, which is another explanation that the peak load at high loading rate is higher than that at low loading rate.

4. Modified fracture energy

The fracture energy (G_f) of the concrete is an important

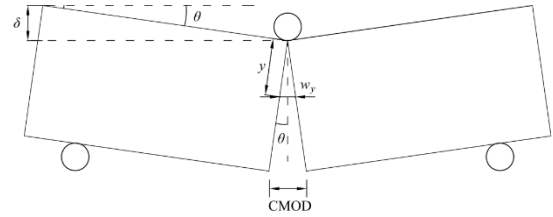


Fig. 13 Dynamic fracture model of three-point flexural beam

fracture mechanics parameter, which can be used to simulate the corresponding crack propagation. Therefore, it is very necessary to establish a detailed method for determining the fracture energy of the concrete.

In order to accurately determine the fracture work (W_f), the concrete specimen in the test should be completely damaged. The fracture energy is calculated by fracture work, and the calculation formula is as follows

$$G_f = \frac{W_f}{b(h-a)} \quad (2)$$

where b and h are the width and height of the concrete specimen respectively, and a is the notch depth.

In this paper, Load-Deflection curve is used to study the fracture energy of the concrete in order to show the relationship between crack opening displacement and the load more intuitively. The Load-Deflection curve can be used as an indirect method to evaluate the fracture energy of the concrete. To obtain the complete fracture energy, the specimens need to be completely destroyed. In the actual test, the MTS testing machine stops working when the specimen has not been completely destroyed. At this time, the specimen still has some residual strain, which makes the Load-Deflection curve incomplete in the experiment, resulting in the calculated fracture energy is smaller than the real one. As shown in Fig. 4, the load tends to zero in the post-peak stage, but the concrete beam does not completely break into two parts, and there is still residual strain, so that the MTS testing machine does not fully record the fracture failure process.

In order to calculate the complete fracture work (W_f) and obtain the exact value of fracture energy (G_f), it is necessary to model the missing part of the tail of Load-Deflection curve. In the final stage of the test, the crack has expanded from the top of the notch to the top of the specimen, and the opening angle of the notch is quite large. In the three-point flexural test, the neutral axis of pressure distribution gradually moves towards the top of the specimen with the decrease of the area of the compression zone. In this case, the three-point flexural beam can be considered as two parts rotating around a point at the top of the mid-span, as shown in Fig. 13.

Therefore, the deflection angle under any deflection (δ) can be calculated through the junction at the top of the concrete beam, and the mathematical formula is as follows

$$\tan \theta = \frac{2\delta}{s} \Rightarrow \theta \approx \frac{2\delta}{s} \quad (3)$$

Then the opening displacement of the notch can be

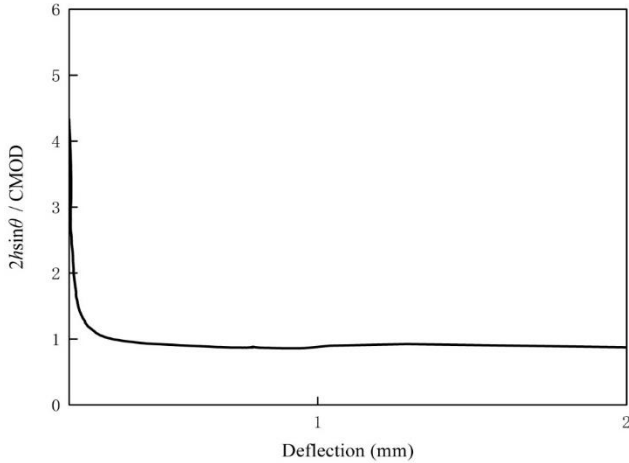


Fig. 14 The comparison of CMOD measured by a clip-on gauge and D_1 calculated by dynamic fracture model (the notch depth is 45 mm)

determined

$$w_y = 2y \sin \theta \approx 2y\theta \quad (4)$$

The opening displacement (D_1) of the notch can be calculated by the dynamic fracture model

$$D_1 = 2h \sin \theta \quad (5)$$

Comparing the CMOD measured by a clip-on gauge with D_1 calculated by the dynamic fracture model, it can be seen that when the ratio of D_1 to CMOD infinitely approaches to 1 as the experiment goes on, that is

$$2h \sin \theta = CMOD \Rightarrow \frac{2h \sin \theta}{CMOD} = 1 \quad (6)$$

It can be considered that the opening displacement of the notch calculated by the dynamic fracture model is accurate.

Fig. 14 verifies the accuracy of the dynamic fracture model when the notch depth is 45 mm (the specimens with the notch depths of 30 mm, 60 mm and 75 mm also show similar rules). It can be concluded that the value of $2h \sin \theta / CMOD$ is about 1 when the deflection of concrete specimen reaches 0.3 mm, and the dynamic fracture model can be proved to be accurate and applicable by Eq. (6).

Hillerborg *et al.* (1976) introduced the cohesive crack model to describe the softening behavior of the post-peak crack of the concrete. Under the assumption of cohesive crack, the concrete specimens show obvious elastic characteristics when the tensile strength (f_t) is not reached. When the concrete specimen generates cracks at a certain point, the stress will be transferred on the crack according to the softening function. As shown in Fig. 15, the crack bridging stress (σ_y) at any point along the crack depth can be expressed as

$$\sigma_y = f(w_y) \quad (7)$$

where w_y is the width of the crack.

For the concrete, the material outside the fracture process zone is linear elastic, but the material in the fracture process zone softens. The softening constitutive curve of

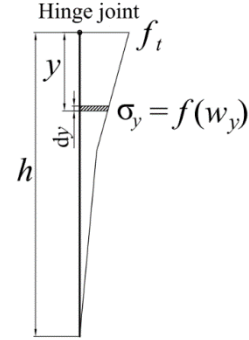


Fig. 15 Stress distribution of dynamic fracture model

the concrete describes the characteristics of the fracture process zone. For plain concrete at room temperature, the softening relationship of the concrete is characterized by the bilinear softening constitutive curve. The moment of dynamic fracture model can be obtained by integrating the product of softening function and specimen width, as shown in Eq. (8)

$$M = \int_0^h b \sigma(w_y) y dy \quad (8)$$

Then it can be obtained from Eq. (4)

$$y = \frac{w_y}{2\theta} \quad (9)$$

Substituting Eq. (9) into Eq. (8) can be obtained

$$M = \frac{b}{(2\theta)^2} \int_0^{w_c} \sigma(w_y) w_y dw_y \quad (10)$$

where w_c represents the crack open displacement when the softening is completed and the stress is 0. The integral part of the Eq. (10) is defined as the parameter A , that is

$$A = \int_0^{w_c} \sigma(w_y) w_y dw_y \quad (11)$$

And substituting Eq. (11) into Eq. (10) can be obtained

$$M = \frac{bA}{(2\theta)^2} \Rightarrow \frac{M}{b} = \frac{A}{(2\theta)^2} \quad (12)$$

Eq. (12) defines the relationship between residual moment of concrete specimen and the rotation angle (θ) when deflection (δ) reaches a critical value. The parameter A can also be determined without defining the shape of the softening curve, because the parameter A is the slope of the curve determined by $(2\theta)^{-2}$ as the abscissa and M/b as the ordinate. Fig. 16 shows the $(2\theta)^{-2}-M/b$ curves of the concrete specimens with different notch depths. As can be seen from the curves, when the deflection is larger (the value of $(2\theta)^{-2}$ is smaller), the parameter A is a constant and can be directly calculated by the slope of the curve. It can be seen from Fig. 16 that although four different curves of concrete specimens with different notch depths have been obtained in the test, their initial slope is almost the same. This indicates that the parameter A is not affected by notch depth but depends on the material properties of the

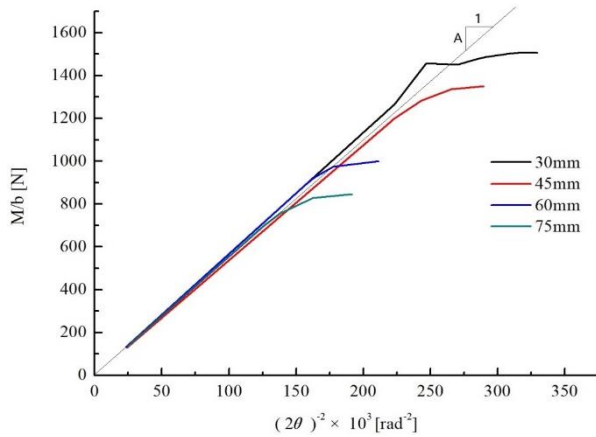


Fig. 16 Determination of parameter K for concrete specimens with different notch depths

concrete. This conclusion is consistent with the view of Bažant. Bažant and Planas (1997) considered that the parameter A is the material property of plain concrete, which is independent of other property.

As shown in Fig. 16, the parameter A of the concrete specimen used in this study is a constant, which is about 0.0058. After determining the parameter A of the material property, the missing part of the Load-Deflection curve can be modeled to accurately determine the fracture energy, and the formula used for tail modeling is as follows

$$P_{stern} = \frac{bsA}{4\delta^2} \quad (13)$$

where b is the width of the concrete beam, s is the span of three-point flexural test, and δ is deflection.

Fig. 17 shows the comparison between the tail model established by Eq. (13) and Load-Deflection curve when the notch depth of the concrete specimen is 30 mm. It can be seen from the figure that the curve obtained by tail modeling is in good agreement with the Load-Deflection curve, which can be used to calculate the tail loss of fracture energy. In addition, the curve obtained by tail modeling can be extended to infinity, which makes up for the deficiency of tail energy loss caused by the test itself. Therefore, the complete fracture work (W_f) of concrete specimen in flexural test can be obtained by the sum of the area enclosed by the Load-Deflection curve and the area enclosed by the curve obtained by tail modeling. The Eq. (14) for calculating fracture work obtained by tail modeling can be given by integral of Eq. (13), as follows

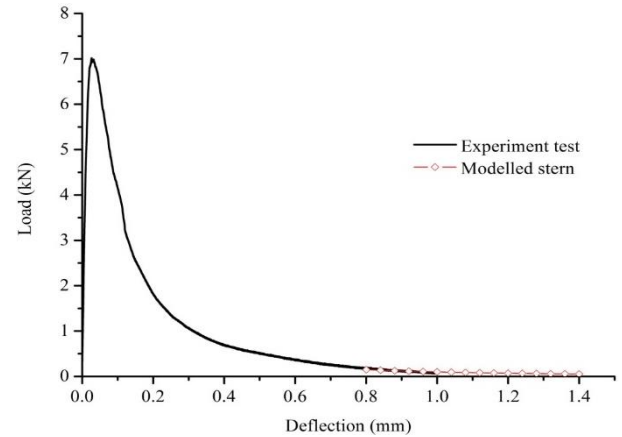


Fig. 17 Comparison between Load-Deflection curve obtained from the test and tail modeling curve

$$W_{stern} = \int_{\delta_{end}}^{\infty} P_{stern} d(\delta) = \frac{bsA}{4\delta_{end}^2} \quad (14)$$

where δ_{end} is the deflection of the last point on the Load-Deflection curve obtained from the test.

Subsequently, the fracture energy of concrete specimens in three-point flexural test can be obtained by Eq. (2). The fracture work (W_f) before modification, the fracture work (W_{stern}) from tail modeling and the fracture energy (G_f) after modification are all calculated by the above fracture mechanics method and the values of them are listed in Table 4.

According to the calculation results, the fracture work (W_{stern}) obtained by the tail-modeling method accounts for about 7.544% of the total fracture work. It can be concluded that this part of the missing fracture work accounts for a relatively large proportion of the total fracture work, which has a greater influence on the accurate measurement of concrete fracture energy. Therefore, it is particularly important to determine the missing work by the tail modeling method. The tail-modeling method can accurately calculate the tail loss of fracture energy of the concrete, thus reducing the calculation error, making the obtained fracture energy more accurate and providing more accurate parameters for the following numerical simulation. It can be concluded from modified fracture energy that the fracture energy (G_f) of the beam increases nonlinearly with the increase of loading rate.

Table 4 Fracture parameters of concrete specimens with different notch depths at different loading rates

Specimen type	Loading rate (mm/s)	A (N·rad ²)	W_f (N·mm)	W_{stern} (N·mm)	G_f (N/mm)	Std.dev. (N/mm)	Specimen number
TPB-30	0.002	0.0058	1252.023	93.039(6.917%)	0.112	0.035	3
TPB-45	0.002	0.0058	938.314	87.634(8.541%)	0.098	0.033	3
TPB-60	0.002	0.0058	855.914	72.957(7.854%)	0.103	0.038	3
TPB-75	0.002	0.0058	570.570	44.230(7.194%)	0.082	0.040	3
TPB-60-1	0.010	0.0058	951.230	74.132(7.230%)	0.114	0.031	3
TPB-60-2	0.002	0.0058	855.914	72.957(7.854%)	0.103	0.038	3
TPB-60-3	0.0002	0.0058	835.913	68.029(7.526%)	0.100	0.037	3

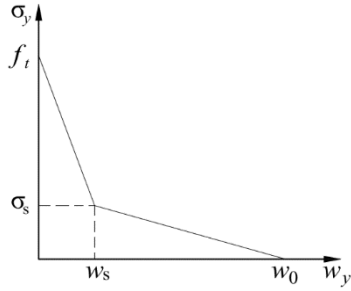


Fig. 18 Bilinear softening constitutive curve of plain concrete

5. Finite element simulation

5.1 Bilinear softening function

In 1976, Hillerborg *et al.* (1976) proposed the virtual crack model, which considered that the fracture process zone (FPZ) at the end of cracks in concrete could be regarded as a virtual stress-transferable crack. The magnitude of the transmissible stress at each point of the crack depends on the deformation value at the point, and the concrete shows corresponding softening characteristics. This characteristic is characterized by the softening constitutive curve of the concrete, which is the basis of many non-linear fracture models. The softening constitutive curve of the concrete under room temperature has been studied extensively by many researchers. Petersson (1981) first proposed the bilinear softening constitutive relationship, and considered that it is more appropriate to simulate the cracking behavior of plain concrete using the bilinear softening function. On the basis of previous studies, CEB-FIP Model Code 1990 (1990), Xu *et al.* (1999) proposed corresponding modified bilinear softening constitutive based on a lot of test studies.

Based on the above research results, the softening cracking behavior of plain concrete was characterized by using the bilinear softening constitutive function at room temperature, taking into account the accuracy and simplicity of calculation. Fig. 18 shows the bilinear softening constitutive function embedded in the finite element model.

When the tensile strength of concrete reaches a certain limit value, the crack begins to develop. The stress required for crack expansion linearly decreases when the crack width increases, and the expression is as follows

$$\sigma_y = f_t - \frac{(f_t - \sigma_s)w_y}{w_0}, 0 \leq w_y \leq w_s \quad (15)$$

where w_y is crack opening displacement; f_t is tensile strength of the concrete at room temperature; and w_0 is the crack opening displacement when the cohesion is 0.

Once the crack width reaches w_s , (w_s, σ_s) is the inflection point of the constitutive curve. Thereafter, the stress decreases with the increase of crack width, but the decrease amplitude is less, and the stress expression is as follows

$$\sigma_y = \frac{\sigma_s(w_0 - w_y)}{w_0 - w_s}, w_s \leq w_y \leq w_0 \quad (16)$$

When the crack width reaches the limit value of w_0 , the stress required for crack propagation decreases to 0, and the stress expression is as follows

$$\sigma_y = 0, w_y \geq w_0 \quad (17)$$

Therefore, the bilinear softening constitutive function of plain concrete is as follows

$$\begin{cases} \sigma_y = f_t - \frac{(f_t - \sigma_s)w_y}{w_0}, 0 \leq w_y \leq w_s \\ \sigma_y = \frac{\sigma_s(w_0 - w_y)}{w_0 - w_s}, w_s \leq w_y \leq w_0 \\ \sigma_y = 0, w_y \geq w_0 \end{cases} \quad (18)$$

In order to simulate the real cracking behavior of plain concrete in finite element model, the modified bilinear softening function of CEB-FIP Model Code 1990 (1990) is used in this paper. The expression is as follows

$$\begin{cases} \sigma_s = 0.15f_t \\ w_s = \frac{G_f}{f_t} - 0.15w_0 \\ w_0 = \frac{\alpha_f G_f}{f_t} \end{cases} \quad (19)$$

where G_f is the modified fracture energy of the concrete obtained by the tail modeling method; and the value of α_f is related to the size of the largest aggregate. Since the maximum aggregate size used in this paper is 20 mm, the value of α_f is 7.

The bilinear softening constitutive function of plain concrete used in this paper can be obtained by substituting Eq. (19) into Eq. (18).

Then, this paper defines the softening constitutive function based on the fracture parameters obtained above and use the finite element simulation to evaluate the prediction performance of the model in the concrete beam with different notch depths.

5.2 Comparative analysis of numerical simulation and experimental results

In order to evaluate the prediction performance of the concrete beams by the softening constitutive model defined by modified fracture energy G_f , the finite element method is used to simulate the concrete beams with different notch

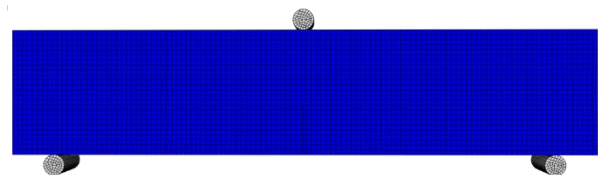


Fig. 19 Finite element model of the concrete beams with the notch

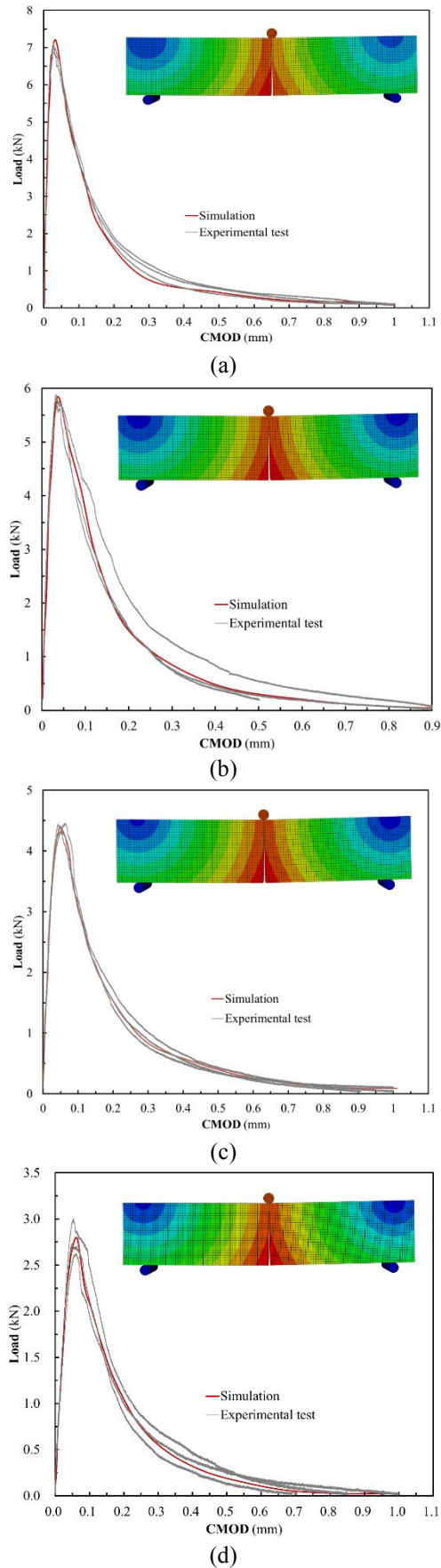


Fig. 20 Comparison of the Load-CMOD curves between finite element simulation and experimental test: (a) $a=30$ mm, (b) $a=45$ mm, (c) $a=60$ mm, (d) $a=75$ mm

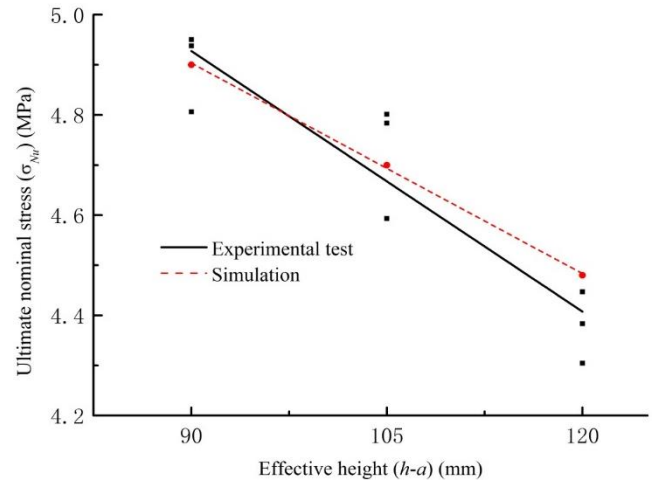


Fig. 21 Comparison of the influence trend of notch depth on ultimate nominal stress σ_{Nu} in experimental test and finite element simulation

depths. According to the size of the concrete beams used in the test, the modified fracture energy was used to establish the finite element model, as shown in Fig. 19. In the model, the maximum principal stress traction cracking criterion is adopted, and the energy-based bilinear softening constitutive model is selected. In order to be consistent with the loading conditions of the test, displacement loading is adopted in the finite element simulation. The displacement is applied to the reference point by coupling the reference point with the loading block. The C3D8R solid element is used in concrete, and an initial notch is prefabricated in the midspan of the beam. Shell element is used in the notch, and grid division is not needed for the notch. The discrete rigid body model is used for loading block.

The fracture modes of the concrete beams with different notch depths under finite element simulation are shown in Fig. 20, and the Load-CMOD curves between the test and numerical simulation are compared. The results show that the Load-CMOD curves obtained by numerical simulation are in good agreement with the experimental curves at different notch depths. This shows that the bilinear softening function determined by the modified fracture energy can be used in ABAQUS to simulate the fracture behavior of the concrete beams more accurately. This conclusion demonstrates that it is reasonable to calibrate the softening function of concrete beams by tail modeling.

In order to further verify that the bilinear softening function determined by the above method can be used in ABAQUS analysis to accurately predict the fracture behavior of concrete beams with different notch depths at different loading rates, the data between numerical simulation and test are compared and analyzed.

Fig. 21 shows the comparison of the influence trend of notch depth on ultimate nominal stress σ_{Nu} between finite element simulation and the test. In order to prove the coincidence between the ultimate nominal stress obtained by finite element simulation and the test results, the size of the specimens used in numerical simulation is consistent with the experimental test. It can be concluded from Fig. 21 that the ultimate nominal stress obtained by finite element

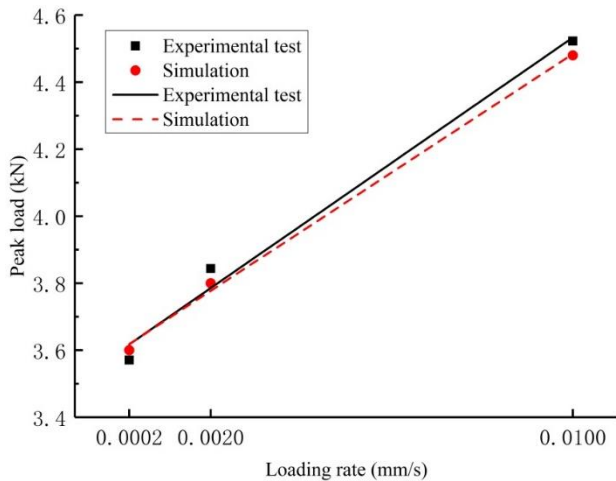


Fig. 22 Comparison of the effects of loading rates on the peak load between experimental test and finite element simulation

simulation is affected by notch depth, which is consistent with the test. This indicates that the finite element analysis can provide a satisfactory prediction for the influence trend of notch depth on concrete beams in test. However, the influence trend of notch depth on the concrete beams in test is more obvious than that of the numerical simulation. Because the numerical simulation only predicts that the fracture energy of the concrete is influenced by the notch depth, but does not consider the boundary layer effect and hydration heat in the process of concrete specimen preparation.

Similarly, Fig. 22 shows the comparison of the influence trend of peak load of the concrete affected by loading rate between numerical simulation and experimental test. Three-point flexural tests for the concrete beams with the notch depth of 60 mm at different loading rates of 0.010 mm/s, 0.002 mm/s and 0.0002 mm/s are simulated by ABAQUS, which are consistent with the test conditions. It can be concluded from numerical simulation results that the peak load of the beam increases with the increase of the loading rates, which are consistent with the test results. And it shows that the bilinear softening function determined by above method can be used in the finite element model to accurately predict the effect of the loading rates on the concrete.

In this paper, bilinear softening constitutive model is established by tail modeling method, and the accuracy of the model to predict the fracture behavior of the concrete beams affected by notch depths and loading rates is verified by finite element simulation. According to the comparative analysis of numerical simulation and experimental results, it can be seen that the bilinear softening function determined by the above method can be used to predict the fracture behavior of concrete beams with different notch depths at different loading rates.

6. Conclusions

In this research, the fracture characteristics of plain

concrete specimens with different notch depths under three-point flexural loads is studied by fracture mechanics and finite element method. The following conclusions are drawn:

The peak load, ultimate nominal stress and ultimate deformation of plain concrete decrease significantly with the increase of the notch depth. This shows that the flexural characteristic of the beams is influenced by notch depth, and its bearing capacity and ductility decrease with the increase of the notch depth. The failure time of the concrete beams is longer when the loading rate is lower. During this period, the cracks generated by loading will extend along the weakest area around the interface transition zone. However, the loading period is shorter when the loading rate is higher, and the cracks will spread directly through the aggregate. Therefore, the strength of concrete beams is higher at higher loading rates.

The strain nephogram of concrete beams at different loading rates and the crack opening width at different heights above the notch are monitored by DIC. It can be seen from the analysis of the monitoring results that strain localization is obvious at pre-peak loading stage under a certain loading rate. Furthermore, the increase of crack length is obviously related to the softening of post-peak loading response. When the loading rate is large, the crack develops along a curve with little curvature, and the curvature of the crack propagation direction increases significantly when the loading rate decreases. The crack opening width increases with the increase of the loading rate. With the increase of crack opening width, the more energy is needed, and the peak load is larger.

It can be seen from the quantitative calculation that the fracture work (W_{stem}) obtained by the tail-modeling method accounts for about 7.544% of the total fracture work. This part of missing fracture work has great influence on the accurate measurement of concrete fracture energy. Therefore, a tail modeling method is proposed to accurately determine the fracture energy of concrete beams, so as to reduce the calculation error and make the fracture of concrete more accurate. In addition, the fracture energy (G_f) of the beam increases nonlinearly with the increase of loading rate.

The fracture energy of the beams is accurately calculated by tail-modeling method, and the bilinear softening constitutive model of flexural fracture behavior is determined. Then, the bilinear softening constitutive function is embedded into the finite element model for numerical simulation. By comparing and analyzing the results of numerical simulation and test, it can be concluded that the influence trend of notch depth on ultimate nominal stress by finite element simulation is consistent with the experimental test. This indicates that the finite element analysis can provide a satisfactory prediction for the influence trend of notch depth on nominal stress in the test. In addition, the influence trend of the loading rates on the peak load of the concrete is consistent with the test results, which indicates that the determined bilinear softening function can be used in the finite element model to predict the influence of loading rates on the peak load. Therefore, the bilinear softening model determined by the tail modeling method can be used in numerical simulation to

predict the fracture behavior of the concrete beams with different notch depths at different loading rates more accurately.

Acknowledgments

This paper is based upon the work supported by the National Natural Science Foundation of China (Grant No. 51979090); Natural Science Foundation for Excellent Young Scholars of Jiangsu Province (Grant No. BK20190075); Young Elite Scientists Sponsorship Program by China Association for Science and Technology (Grant No. 2017QNRC001).

References

- Abbass, W., Siddiqi, Z.A., Aslam, F., Hussain, R.R. and Ahmed, S. (2013), "Bond behaviour of high-strength concrete flexural member under low cyclic fatigue loading", *Fatig. Fract. Eng. Mater. Struct.*, **36**(7), 602-613. <https://doi.org/10.1111/ffe.12027>.
- Ali-Ahmad, M., Subramaniam, K. and Ghosn, M. (2006), "Experimental investigation and fracture analysis of debonding between concrete and FRP sheets", *J. Eng. Mech.*, **132**(9), 914-923. [https://doi.org/10.1061/\(ASCE\)0733-9399\(2006\)132:9\(914\)](https://doi.org/10.1061/(ASCE)0733-9399(2006)132:9(914)).
- Bazant, Z.P. and Planas, J. (1997), *Fracture and Size Effect in Concrete and Other Quasi-Brittle Materials*, CRC Press LLC, Boca Raton.
- Carlioni, C. and Subramaniam, K.V. (2010), "Direct determination of cohesive stress transfer during debonding of FRP from concrete", *Compos. Struct.*, **93**(1), 184-192. <https://doi.org/10.1016/j.compstruct.2010.05.024>.
- Carlioni, C. and Subramaniam, K.V. (2013), "Investigation of sub-critical fatigue crack growth in FRP/concrete cohesive interface using digital image analysis", *Compos Part B-Eng.*, **51**, 35-43. <https://doi.org/10.1016/j.compositesb.2013.02.015>.
- CEB-Comite Euro-international du Beton (1990), CEB-FIP model code 1990, Bulletin D' information. No.213/214[S].
- Chen, H.H.N., Su, R.K.L., Fok, S.L. and Zhang, H.G. (2017), "Fracture behavior of nuclear graphite under three-point bending tests", *Eng. Fract. Mech.*, **186**, 143-157. <https://doi.org/10.1016/j.engfracmech.2017.09.030>.
- Duan, K., Hu X. and Wittmann F.H. (2006), "Scaling of quasi-brittle fracture: boundary and size effect", *Mech. Mater.*, **38**(1-2), 128-141. <https://doi.org/10.1016/j.mechmat.2005.05.016>.
- Earij, A., Alfano, G., Cashell, K. and Zhou, X.M. (2017), "Nonlinear three-dimensional finite-element modelling of reinforced-concrete beams: Computational challenges and experimental validation", *Eng. Fail. Anal.*, **82**, 92-115. <https://doi.org/10.1016/j.engfailanal.2017.08.025>.
- Elices, M., Guine, G.V. and Planas, J. (1997), "On the measurement of concrete fracture energy using three-point bend tests", *Mater. Struct.*, **30**(200), 375-376. <https://doi.org/10.1007/BF02480689>.
- Firoozi, S., Dehestani, M. and Neya, B.N. (2018), "Effect of water to cement ratio on the mode III fracture energy of self-compacting concrete", *Mater. Struct.*, **51**(4), 80. <https://doi.org/10.1617/s11527-018-1208-x>.
- Gang, H. and Kwak, H.G. (2017), "A tensile criterion to minimize FE mesh-dependency in concrete beams under blast loading", *Comput. Concrete*, **20**(1), 1-10. <https://doi.org/10.12989/cac.2017.20.1.001>.
- Haeri H. (2015), "Simulating the crack propagation mechanism of pre-cracked concrete specimens under shear loading conditions", *Strength Mater.*, **47**(4), 618-632. <https://doi.org/10.1007/s11223-015-9698-z>.
- Haeri, H. and Sarfarazi V. (2016), "Numerical simulation of tensile failure of concrete using particle flow code (PFC)", *Comput. Concrete*, **18**(1), 39-51. <https://doi.org/10.12989/cac.2016.18.1.039>.
- Haeri, H., Shahriar, K. and Marji, M.F. (2013), "Modeling the propagation mechanism of two random micro cracks in rock samples under uniform tensile loading", *13th International Conference on Fracture*.
- Hillerborg, A., Modeer, M. and Petersson, P.E. (1976), "Analysis of crack formation and crack growth in concrete by means of fracture mechanics and finite elements", *Cement Concrete Res.*, **6**(6), 773-782. [https://doi.org/10.1016/0008-8846\(76\)90007-7](https://doi.org/10.1016/0008-8846(76)90007-7).
- Karamloo, M. and Mazloom, M. (2018), "An efficient algorithm for scaling problem of notched beam specimens with various notch to depth ratios", *Comput. Concrete*, **22**(1), 39-51. <https://doi.org/10.12989/cac.2018.22.1.039>.
- Li, D.Y., Huang, P.Y., Guo, X.Y., Zheng, X.H., Lin, J.X. and Chen, Z.B. (2018), "Fatigue crack propagation behavior of RC beams strengthened with CFRP under cyclic bending loads", *Fatig. Fract. Eng. Mater. Struct.*, **41**(1), 212-222. <https://doi.org/10.1111/ffe.12673>.
- Navalurkar, R.K. and Hsu, C.T.T. (2001), "Fracture analysis of high strength concrete members", *J. Mater. Civil Eng.*, **13**(3), 185-193. [https://doi.org/10.1061/\(ASCE\)0899-1561\(2001\)13:3\(185\)](https://doi.org/10.1061/(ASCE)0899-1561(2001)13:3(185)).
- Ohno, K., Uji, K., Ueno, A. and Ohtsu, M. (2014), "Fracture process zone in notched concrete beam under three-point bending by acoustic emission", *Constr. Build. Mater.*, **67**, 139-145. <https://doi.org/10.1016/j.conbuildmat.2014.05.012>.
- Petersson, P.E. (1981), "Crack growth and development of fracture zones in plain concrete and similar materials", Report TVBM-1006[R], Lund Institute of Technology, Division of Building Materials, Sweden.
- Rama, J.S.K., Chauhan, D.R., Sivakumar, M.V.N., Vasani, A. and Murthy, A.R. (2017), "Fracture properties of concrete using damaged plasticity model-A parametric study", *Struct. Eng. Mech.*, **64**(1), 59-69. <https://doi.org/10.12989/sem.2017.64.1.059>.
- Ranade, R., Li, V.C. and Heard, W.F. (2015), "Tensile rate effects in high strength-high ductility concrete", *Cement Concrete Res.*, **68**, 94-104. <https://doi.org/10.1016/j.cemconres.2014.11.005>.
- Reinhardt, H.W. and Cornelissen, H.A.W. (1986), "Tensile

- tests and failure analysis of concrete”, *J. Struct. Eng.*, **112**(11), 2462-2477. [https://doi.org/10.1061/\(ASCE\)0733-9445\(1986\)112:11\(2462\)](https://doi.org/10.1061/(ASCE)0733-9445(1986)112:11(2462)).
- Reinhardt, H.W. and Ozbolt, J. (2007), “Fracture of concrete beams at different loading rates”, *Fract. Mech. Concrete Concrete Struct.*, **1-3**, 563-569.
- Robins, P., Austin, S., Chandler, J. and Jones, P. (2001), “Flexural strain and crack width measurement of steel-fibre-reinforced concrete by optical grid and electrical gauge methods”, *Cement Concrete Res.*, **31**(5), 719-729. [https://doi.org/10.1016/S0008-8846\(01\)00465-3](https://doi.org/10.1016/S0008-8846(01)00465-3).
- Sarfarazi V. and Haeri H. (2016), “A review of experimental and numerical investigations about crack propagation”, *Comput. Concrete*, **18**(2), 235-266. <http://dx.doi.org/10.12989/cac.2016.18.2.235>.
- Sasmal, S., Thiyagarajan, R., Lieberum, K.H. and Koenders, E.A.B. (2018), “Numerical simulations of progression of damage in concrete embedded chemical anchors”, *Comput. Concrete*, **22**(4), 395-405. <https://doi.org/10.12989/cac.2018.22.4.395>.
- Shang, S.M. and Song, Y.P. (2013), “Dynamic biaxial tensile-compressive strength and failure criterion of plain concrete”, *Constr. Build. Mater.*, **40**, 322-329. <https://doi.org/10.1016/j.conbuildmat.2012.11.012>.
- Skarzynski, L., Nitka, M. and Tejchman, M. (2015), “Modelling of concrete fracture at aggregate level using FEM and DEM based on X-ray μ CT images of internal structure”, *Eng. Fract. Mech.*, **147**, 13-35. <https://doi.org/10.1016/j.engfracmech.2015.08.010>.
- Subramaniam, K.V., Carloni, C. and Nobile, L. (2007), “Width effect in the interface fracture during shear debonding of FRP sheets from concrete”, *Eng. Fract. Mech.*, **74**(4), 578-594. <https://doi.org/10.1016/j.engfracmech.2006.09.002>.
- Subramaniam, K.V., Nakale, S. and Gali, S. (2015), “Investigation of crack propagation in macro-synthetic fiber reinforced concrete”, *5th International Conference on Construction Materials: Performance, Innovations and Structural Implications*, Whistler, Canada.
- Travas, V., Ozbolt, J. and Kozar, I. (2009), “Failure of plain concrete beam at impact load: 3D finite element analysis”, *Int. J. Fract.*, **160**(1), 31-41. <https://doi.org/10.1007/s10704-009-9400-1>.
- Trivedi, N., Singh, R.K. and Chattopadhyay, J. (2015), “Size independent fracture energy evaluation for plain cement concrete”, *Fatig. Fract. Eng. Mater. Struct.*, **38**(7), 789-798. <https://doi.org/10.1111/ffe.12283>.
- Xiao, J., Liu, Q. and Wu, Y.C. (2012), “Numerical and experimental studies on fracture process of recycled concrete”, *Fatig. Fract. Eng. Mater. Struct.*, **35**(8), 801-808. <https://doi.org/10.1111/j.1460-2695.2012.01673.x>.
- Xu, S.L. and Reinhardt, H.W. (1999), “Determination of double-K criterion for crack propagation in quasi-brittle fracture, Part II: Analytical evaluating and practical measuring methods for three-point bending notched beam”, *Int. J. Fract.*, **98**(2), 151-177. <https://doi.org/10.1023/A:1018740728458>.
- Yan, D.M., Lin, G. and Chen, G.D. (2009), “Dynamic properties of plain concrete in triaxial stress state”, *ACI Mater. J.*, **106**(1), 89-94.
- Zhang, X.X., Elazim, A., Ruiz, G. and Yu, R.C. (2014), “Fracture behavior of steel fibre-reinforced concrete at a wide range of loading rates”, *Int. J. Impact Eng.*, **71**, 89-96. <https://doi.org/10.1016/j.ijimpeng.2014.04.009>.

HK